Strong interaction and *E*2 effect in even-*A* antiprotonic Te atoms

B. Kłos
Physics Department, Silesian University, PL-40-007 Katowice, Poland

S. Wycech
Sołtan Institute for Nuclear Studies, PL-00-681 Warsaw, Poland

A. Trzcińska, J. Jastrzębski, T. Czosnyka, M. Kisieliński, P. Lubiński,* P. Napiorkowski, and L. Pieńkowski
Heavy Ion Laboratory, Warsaw University, PL-02-093 Warsaw, Poland

F. J. Hartmann, B. Ketzer, R. Schmidt, and T. von Egidy
Physik-Department, Technische Universität München, D-85748 Garching, Germany

J. Cugnon
Institut de Physique, Universite de Liege au Sart Tilman, B4000 Liege 1, Belgium

K. Gulda and W. Kurcewicz
Institute of Experimental Physics, Warsaw University, PL-00-681 Warsaw, Poland

E. Widmann[†]
CERN, CH-1211 Geneva 23, Switzerland
(Received 17 October 2003; published 19 April 2004)

The x-ray cascade from antiprotonic atoms was studied for ^{122}Te, ^{124}Te, ^{126}Te, ^{128}Te, and ^{130}Te. Widths and shifts due to the strong interaction were deduced for several levels. The *E*2 nuclear resonance effect was observed in all investigated nuclei. In ^{130}Te the *E*2 resonance allowed to determine level widths and shifts of the *LS*-split deeply bound $(n,l)=(6,5)$ state, otherwise unobservable. The measured level widths and shifts, corrected for the *E*2-resonance effect, were used to investigate the nucleon density in the nuclear periphery. The deduced neutron distributions are compared with results of the previously introduced radiochemical method and with Hartree-Fock-Bogoliubov model calculations.

I. INTRODUCTION

The present paper reports part of our systematic study of heavy antiprotonic atoms undertaken during the last two years of the Low Energy Antiproton Ring (LEAR) activity at CERN. Although the most important part of the antiprotonic x-ray data (level widths and shifts) was already briefly reported [1,2] and analyzed [3]—a number of experimental results and their interpretation were also given in Refs. [4–6] and will be a subject of more exhaustive articles.

The experimental study of the antiprotonic atoms of a series of even-*A* tellurium isotopes was motivated first by the prediction of a strong *E*2-resonance effect [7] in ^{130}Te, which would allow us to obtain information on the properties of a deeply bound, "hidden" antiprotonic level, inaccessible by the antiprotonic cascade. The investigation of the *E*2-resonance effect occurring in this isotope was previously reported in Ref. [8]. In that reference the attenuation coeffi-

cient of the $n=8 \rightarrow n=7$ x-ray transition affected by the resonance was determined but this did not allow the authors to deduce the width and shift of the $n=8$ level in a unique way. When undertaking the present investigation it was hoped that the comparison of a series of even-*A* tellurium isotopes can lead to a precise determination of both these observables. This, in turn, would allow us to deduce the widths and shifts of the deeply bound $n=6$ level in ^{130}Te which are more strongly dependent on the antiproton-nucleus interaction than are levels directly populated by the antiprotonic cascade.

A second motivation for the study of even antiprotonic Te atoms was the search for isotope effects in the level widths and shifts. As in other isotopic chains investigated by our collaboration these effects would be a sign of changes in the nuclear periphery when pairs of neutrons are added to the lightest isotope studied—in our case ^{122}Te. Tellurium nuclei have only two protons outside the closed $Z=50$ shell and their study constitutes a natural extension to our previous investigation of the isotope effects in even Sn nuclei [6].

This paper is organized as follows. Section II presents very briefly the experimental procedure with reference to our previous papers where a more detailed description was given. The experimental results are presented in Sec. III. Data analysis and discussion in Sec. IV are divided into two

---

*Present address: N. Copernicus Astronomical Center, Pl-00-716 Warsaw, Poland.

†Present address: Department of Physics, University of Tokyo, 7-3-1 Hongo, Bunkyo-ku, Tokyo 113-0033, Japan.

69 044311-1

TABLE I. Target properties.

Target	Thickness d (mg/cm^2)	Enrichment (%)	Number of $\bar{p}$ (10^8)
^{122}Te	96.2	92.8	13
^{124}Te	301.8	90.7	11
^{126}Te	96.4	98.1	11
^{128}Te	353.4	98.2	13
^{130}Te	248.2	99.4	20

parts. The first one analyzes the *E2* nuclear resonance effects in tellurium isotopes, whereas in the second one the *E2* corrected level shifts and widths are used to determine the neutron distribution in the periphery of the investigated nuclei. Section V summarizes and concludes this paper.

II. THE EXPERIMENT

Five even-*A* tellurium isotopes were investigated during two experiments conducted in 1995 and 1996. In 1995 the antiprotonic atoms of ^{124}Te, ^{128}Te, and ^{130}Te were studied using antiprotons with a momentum of 300 MeV/c. The isotopes of ^{122}Te and ^{126}Te were investigated in 1996 using a beam of 106 MeV/c antiprotons. Table I gives the target properties and the number of antiprotons used for each target.

The antiprotonic x rays were measured with high purity germanium (HPGe) detectors. In 1995 one planar detector with 25 mm diameter and 13 mm thickness was employed. One coaxial detector with an active diameter of 49 mm and a length of 49.5 mm (relative efficiency about 19%) and one planar detector with 36 mm diameter and 14 mm thickness were used in 1996.

More details concerning the experimental methods, the detector calibration, and the data reduction may be found in
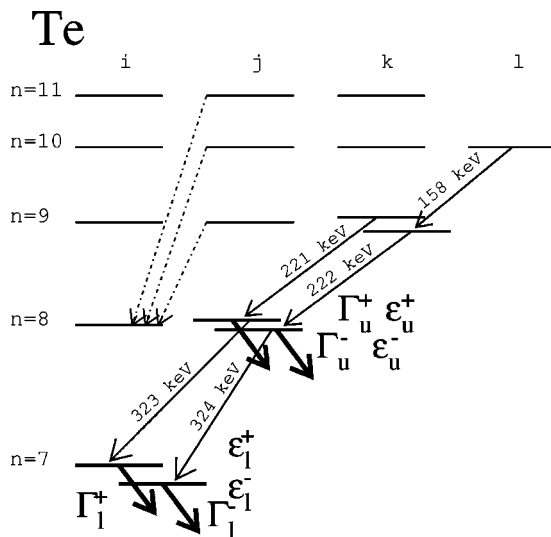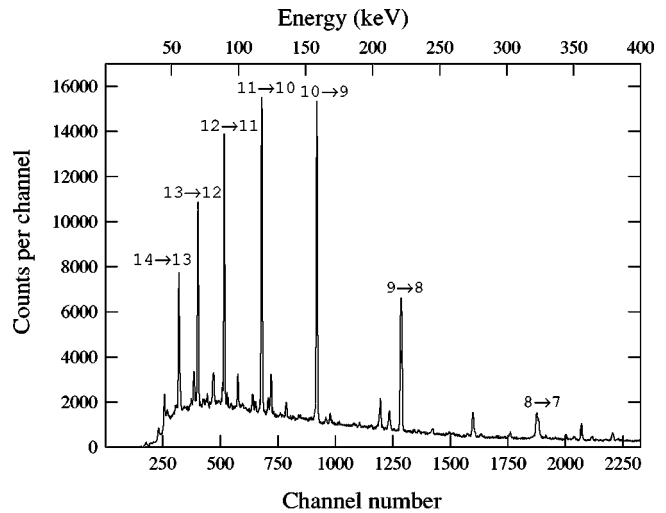

FIG. 2. Antiprotonic x-ray spectrum from ^{122}Te measured with the HPGe detector of 19% relative efficiency.

our previous publications [4–6]. We also refer to these publications for an introduction to the phenomena relevant for the antiprotonic cascade and strong interaction affecting the last observable x-ray transitions.

III. EXPERIMENTAL RESULTS

The strong interaction between antiproton and nucleus causes a sizeable change of the energy of the last x-ray transition from its purely electromagnetic value. The nuclear absorption reduces the lifetime of the lowest accessible atomic state (the "lower level," which for tellurium is the $n=7$ state) and hence the x-ray line is broadened. Nuclear absorption also occurs from the next higher level ("upper level") although the effects on level energy and width are generally too small to be directly measured. The width of the $(n,l=8,7)$ level was deduced indirectly by measuring the loss of
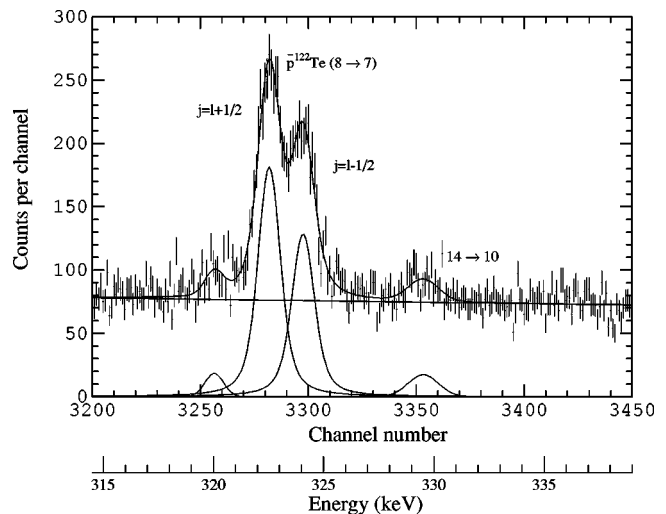

FIG. 1. Level scheme for antiprotonic tellurium atom. The observables of the present experiment are indicated.

FIG. 3. Part of the antiprotonic x-ray spectrum measured for ^{122}Te using the detector with the 1035×14 mm^3 crystal. The fit to the broadened 8→7 line is also shown.

TABLE II. Measured relative x-ray intensities normalized to the transition $n=10 \rightarrow n=9$.

Transition	Energy (keV)	^{122}Te	^{124}Te	^{126}Te	^{128}Te	^{130}Te
$8 \rightarrow 7$	323.4	38.0±2.4	48.4±3.5	44.7±2.7	40.5±3.2	14.1±1.8
$9 \rightarrow 8$	221.3	74.0±2.8	95.9±4.8	95.3±3.6	105.1±5.4	101.9±6.0
$10 \rightarrow 9$[a]	158.2	100.0±5.3	100.0±7.2	100.0±5.7	100.0±7.3	100.0±8.0
$11 \rightarrow 10$	117.0	92.6±4.7	86.1±5.8	93.5±4.7	84.7±5.9	83.9±6.6
$12 \rightarrow 11$	88.9	78.3±4.0		79.2±4.0		
$13 \rightarrow 12$	69.1	64.5±3.4		65.6±3.3		
$14 \rightarrow 13$	54.8	60.8±3.1		62.6±3.2		
$9 \rightarrow 7$	544.7	3.1±0.4				7.4±1.1
$10 \rightarrow 8$	379.5	8.1±0.5	9.8±1.0	7.7±0.6	9.0±0.8	8.7±0.8
$11 \rightarrow 9$	275.2	12.5±1.1	13.2±2.6	10.3±0.8	12.8±1.3	12.1±1.4
$12 \rightarrow 10$	205.9	11.8±0.7	13.5±1.0	13.0±0.7	13.5±1.0	13.6±1.1
$13 \rightarrow 11$[a]	158.0	13.3±0.7	15.2±1.0	13.6±0.8	12.9±1.0	13.0±1.0
$14 \rightarrow 12$	123.9	12.3±0.7	12.5±0.9	13.3±0.7	11.8±0.9	11.9±1.0
$15 \rightarrow 13$	99.1	10.4±0.6		10.2±0.6		
$16 \rightarrow 14$	80.4	6.3±0.4		7.0±0.6		
$17 \rightarrow 15$	66.1	9.7±0.5		10.2±0.5		
$10 \rightarrow 7$	702.9	2.4±0.4				
$11 \rightarrow 8$	496.5	2.2±0.4				
$12 \rightarrow 9$	364.1	3.0±0.3	3.7±0.6	3.1±0.3	3.4±0.5	2.4±0.4
$13 \rightarrow 10$	275.0	4.0±0.4	4.0±0.5	4.5±0.4	4.4±0.3	4.1±0.4
$14 \rightarrow 11$	212.8	8.9±0.5[b]	4.5±0.5	4.8±0.3	4.4±0.4	3.9±0.4
$15 \rightarrow 12$	168.2	3.1±0.2	3.2±0.3	3.7±0.3	3.6±0.3	3.4±0.3
$16 \rightarrow 13$	135.2	2.3±0.3	2.7±0.4	3.5±0.3	2.1±0.5	2.5±0.4
$17 \rightarrow 14$	110.3	5.0±0.3	6.1±0.5	4.7±0.3	6.0±0.5	5.7±0.5
$18 \rightarrow 15$	91.2	3.9±0.2		4.0±0.2		
$12 \rightarrow 8$	585.4	1.6±0.4				
$13 \rightarrow 9$	433.2	1.4±0.2				
$14 \rightarrow 10$	329.8	1.6±0.1	2.0±0.1	1.7±0.1	2.1±0.2	1.7±0.2
$15 \rightarrow 11$	257.1	1.6±0.1	1.7±0.2	2.0±0.3	1.9±0.2	1.8±0.2
$16 \rightarrow 12$	204.3	1.6±0.2	1.3±0.2	2.1±0.2	1.5±0.2	1.9±0.2
$17 \rightarrow 13$	165.1	1.7±0.2	1.9±0.2	2.3±0.2	2.2±0.2	2.0±0.2
$18 \rightarrow 14$	135.4	2.0±0.2	2.2±0.2	2.1±0.2	2.4±0.2	1.8±0.3
$19 \rightarrow 15$	112.4	2.9±0.2	2.7±0.2	1.9±0.2	2.4±0.2	1.9±0.2

[a]The $10 \rightarrow 9$ and $13 \rightarrow 11$ transition intensity ratio was obtained from antiprotonic cascade calculations performed with a modified statistical initial distribution $[p(l) \propto 2(l+1)\exp(\alpha \cdot l); \alpha \approx 0.1]$ [4].
[b]The antiprotonic x-ray line is mixed with a strong nuclear $3/2^+ \rightarrow 1/2^+$ transition in ^{121}Te ($N_{target}-1$ isotope, see Ref. [18]).

intensity of the final x-ray transitions. The level scheme for the tellurium antiprotonic atoms with the observables of the x-ray experiment is shown in Fig. 1.

The x-ray spectrum measured with antiprotons stopped in ^{122}Te is shown in Fig. 2. Those lines in the spectra that are not broadened were fitted with Gaussian profiles. The lowest observable *LS*-split doublet lines ($n=8 \rightarrow 7$), which are sig-

nificantly broadened, were fitted with two Lorentzians convoluted with Gaussians (Fig. 3). The experimental resolution also allowed to resolve two Gaussian-shaped, *LS*-split $n=9 \rightarrow 8$ lines.

The measured relative intensities of the antiprotonic x rays observed in all investigated tellurium targets are given in Table II. These intensities were used to determine the
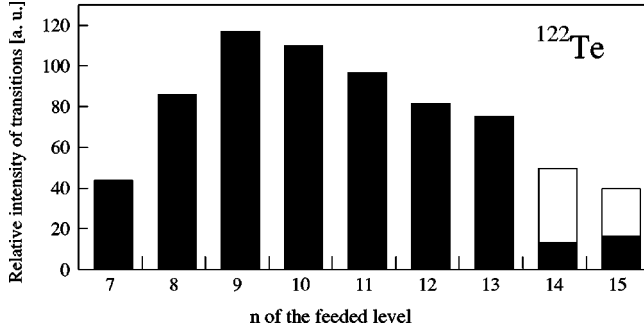
FIG. 4. Total relative intensities of observed transitions (normalized to the transition $n=10 \rightarrow n=9$, taken as 100) feeding the indicated n level in ^{122}Te. The transitions not observed experimentally come from a cascade calculation (open area). The decrease in intensity of the transitions feeding the $n=8$ level is due to the $E2$-resonance effect (see text and Fig. 5).

feeding of the consecutive n levels along the antiprotonic cascade. This is shown in Fig. 4.

Table III gives the measured shifts ε defined by $\varepsilon = E_{em} - E_{expt}$, where E_{expt} is the experimental value for the transition energy and E_{em} is the energy calculated without strong interaction [9]. For the $n,l=7,6$ levels the shifts are clearly repulsive, whereas for the $n,l=8,7$ levels they are compatible with zero except for ^{128}Te and ^{130}Te, where the upper levels are affected by the $E2$ resonance. Tables IV and V give the measured widths. As indicated above, the widths of the $n,l=8,7$ levels were derived from the intensity balance of transitions feeding and depopulating these levels. Contributions of parallel transitions to the measured intensities were obtained from cascade calculations (see Ref. [4]). The rates for radiative dipole transitions were calculated from the formulas given in Ref. [10]. The Auger rates were derived from the radiative rates and from cross sections for the photoeffect using Ferrell's formula [11]. The width of the level $n,l=8,7$ for ^{130}Te, and to a smaller extent that for ^{128}Te, is larger than in the other tellurium isotopes. This is due to the $E2$ nuclear resonance effect to be discussed below. Besides this effect the data of Tables III–V hardly show any systematic changes in shifts or widths in the whole series of tellurium isotopes. At first glance this seems strange: the heaviest tellurium isotope studied has eight neutrons more than the lightest one and, from our study of Sn isotopes [6], isotope effects in shifts and widths would be expected. As it will be shown in the following sections, the additional neu-

tron contributions to the level widths and shifts are in the tellurium isotopic chain counterbalanced by the deformation effect (the deformation decreases with increasing mass number A).

IV. DATA ANALYSIS AND DISCUSSION

A. The $E2$-resonance effects—observation of a deeply bound $\bar{p}$ state

Nuclear deformation affects the atomic levels mainly due to the quadrupole interaction between the atomic and the nuclear system [7]. It is described by the Hamiltonian

$$H_Q = -\frac{e^2}{2r^3} Q_{2\mu} Y_{2\mu}, \qquad (1)$$

where $Q_{2\mu}$ is the nuclear quadrupole operator and $Y_{2\mu}$ is a spherical harmonic in the antiproton coordinates. This potential mixes atomic and nuclear states, and the mixing matrix $\langle n,l,0^+|H_Q|n',l',2^+ \rangle$ connects the 0^+ nuclear ground state to the first excited 2^+ state. These mixing matrix elements are particularly large in the $n'=n-2$ and $l'=l-2$ cases of the circular ($l=n-1$) orbits. This concentration of strength is a consequence of the quadrupole nature of H_Q and the nodeless radial atomic wave functions for the circular orbits.

The $|n=8,l=7;0^+\rangle$ states in tellurium are mixed with the $|n=6,l=5;2^+\rangle$ states (see Fig. 5). The values of the mixing matrix are close to 1 keV and the level spacing between these two states is about 15 keV. The small ratio of mixing strength and level spacing allows a perturbative treatment and the $E2$-induced, complex energy shift due to this mixing is approximately given by

TABLE IV. Measured absorption widths $\Gamma_l^\pm$ of the $n,l=7,6$ level in the antiprotonic tellurium atoms (the $\pm$ sign corresponds to the $j=l\pm1/2$ orbit).

Target	Γ_l^+ (eV)	Γ_l^- (eV)
^{122}Te	583 ± 77	661 ± 77
^{124}Te	562 ± 68	532 ± 76
^{126}Te	624 ± 73	683 ± 72
^{128}Te	546 ± 87	722 ± 82
^{130}Te	604 ± 138	707 ± 201

TABLE III. Measured shifts $\varepsilon_u^\pm$ of the $n,l=8,7$ (upper) and $\varepsilon_l^\pm$ of the $n,l=7,6$ (lower) levels in the antiprotonic tellurium atoms (the $\pm$ sign corresponds to the $j=l\pm1/2$ orbit).

Target	ε_u^+ (eV)	ε_u^- (eV)	ε_l^+ (eV)	ε_l^- (eV)
^{122}Te	3 ± 11	-7 ± 11	52 ± 35	50 ± 45
^{124}Te	-3 ± 7	-6 ± 7	48 ± 21	55 ± 27
^{126}Te	4 ± 10	6 ± 11	56 ± 34	31 ± 45
^{128}Te	18 ± 6	12 ± 6	52 ± 20	79 ± 31
^{130}Te	-56 ± 5	-80 ± 5	46 ± 42	89 ± 73

TABLE V. Radiation width Γ_{em} and Auger width Γ_{Auger} for the $n=8$ levels, where the strong interaction width Γ_u was determined via the intensity balance.

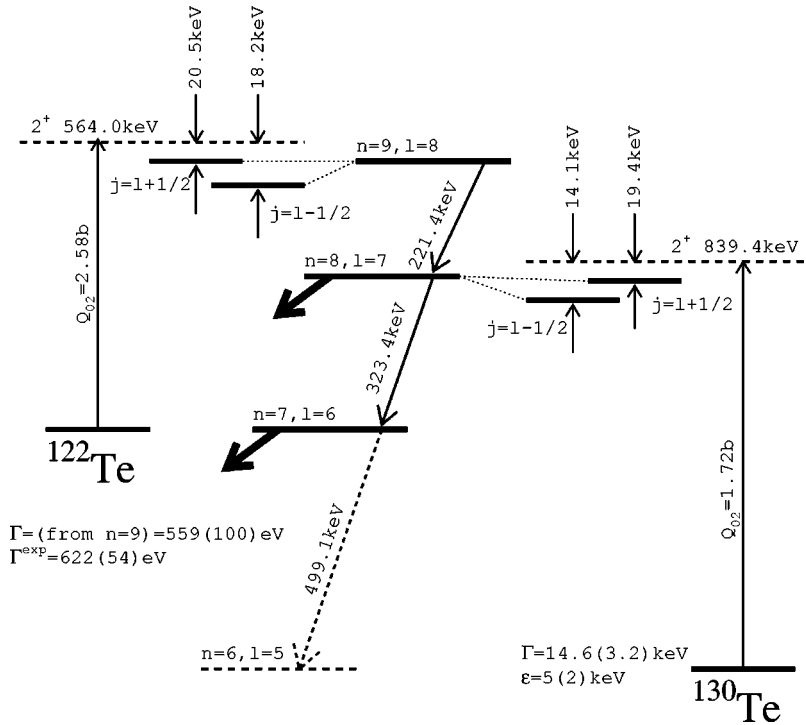| Target	Γ_{em} (eV)	Γ_{Auger} (eV)	Γ_u^+ (eV)	Γ_u^- (eV)
^{122}Te	6.60	0.043	7.1 ± 1.4	8.0 ± 1.3
^{124}Te	6.54	0.042	6.6 ± 1.6	8.6 ± 1.8
^{126}Te	6.48	0.042	7.9 ± 1.1	8.9 ± 1.5
^{128}Te	6.42	0.042	10.9 ± 2.3	11.4 ± 2.5
^{130}Te	6.37	0.041	36 ± 9	52 ± 16

FIG. 5. The antiprotonic-atom level energies and corresponding nuclear excitations of the 2^+ states in ^{122}Te and ^{130}Te.

$$\varepsilon(E2;8,7) - i\frac{\Gamma(E2;8,7)}{2} \cong \frac{\langle 8,7;0^+|H_Q|6,5;2^+\rangle^2}{E(8,7;0^+) - E(6,5;2^+)}, \quad (2)$$

where $E(8,7;0^+)$ is the energy of the $|n=8,l=7;0^+\rangle$ state and $E(6,5;2^+)=E(2^+)+E_{em}(6,5)+\varepsilon(6,5)-i\Gamma(6,5)/2$ is the energy of the atom in the $|n=6,l=5\rangle$ state and the nucleus in the 2^+ state. The energy $E(6,5;2^+)$ contains a complex level shift of the admixed level which is not accessible by direct atomic cascade transitions. The interest in this state stems from the fact that it offers the largest nuclear-atomic overlap tested so far with antiprotonic atoms. The real situation is slightly more complicated than that indicated in Eq. (2) since the two states of interest are split into the $j=l+1/2$ (upper) and $j=l-1/2$ (lower) fine structure (fs) components. Thus there are three mixing matrix elements involved. The two elements that mix the corresponding *upper-upper* and *lower-lower* fs components[1] of

each (n,l) doublet are large (1.135 and 1.150 keV in ^{130}Te). The third one that mixes the lower-upper components of the corresponding doublets is weaker (0.18 keV). The method is described in more detail in Refs. [7,8], and for the explicit representation of these matrix elements we refer to the review of Ref. [12].

The $E2$ nuclear resonance effect occurs when an atomic deexcitation energy closely matches a nuclear excitation energy and the electric quadrupole coupling induces configuration mixing. Such an effect is noticeable in antiprotonic ^{122}Te and ^{128}Te, and is large in ^{130}Te. The cases of ^{122}Te and ^{130}Te are illustrated in Fig. 5. In ^{130}Te the spacing between the antiprotonic $(n,l)=(8,7)$ and $(6,5)$ levels (820.0 keV for the upper and 825.3 keV for the lower fs states) is sufficiently close to the first $I^\pi=2^+$ nuclear excitation energy (839.4 keV) to allow a sizable configuration mixing of the $|8,7;0^+\rangle$ and $|6,5;2^+\rangle$ atomic nuclear states. First we discuss

TABLE VI. Shifts of the $n,l=8,7$ states.

Isotope	Experimental (eV)		$E2$ induced (eV)		Optical (eV)	
	$j=l+1/2$	$j=l-1/2$	$j=l+1/2$	$j=l-1/2$	$j=l+1/2$	$j=l-1/2$
^{122}Te	3(11)	−7(12)	12	12	−9(11)	−19(12)
^{124}Te	−3(7)	−6(7)	12	12	−15(7)	−18(7)
^{126}Te	4(10)	6(11)	14	14	−10(10)	−8(11)
^{128}Te	18(6)	12(6)	24	22	−6(6)	−10(6)
^{130}Te	−56(5)	−80(5)	−46(6)	−67(6)	−10(4)[a]	−13(4)[a]

[a]Values for ^{130}Te are obtained by an extrapolation from ^{122}Te-^{128}Te.

---

[1]To avoid confusion we denote fs components by (+) and (−).

TABLE VII. Widths of $n,l=8,7$ levels.

Isotope	Experimental (eV)		$E2$ induced (eV)		Optical (eV)	
	$j=l+1/2$	$j=l-1/2$	$j=l+1/2$	$j=l-1/2$	$j=l+1/2$	$j=l-1/2$
^{122}Te	7.1(1.4)	8.0(1.3)	0.8	0.5	6.3(1.4)	7.5(1.3)
^{124}Te	6.6(1.6)	8.6(1.8)	1.0	0.6	5.6(1.6)	8.0(1.8)
^{126}Te	7.9(1.1)	8.9(1.5)	1.7	1.0	6.2(1.1)	7.9(1.5)
^{128}Te	10.9(2.3)	11.4(2.5)	5.8	3.3	5.1(2.3)	8.2(2.5)
^{130}Te	36(9)	52(16)	30(9)	44(16)	6.0(0.7)[a]	7.8(0.8)[a]

[a]Values for ^{130}Te are obtained by an extrapolation from ^{122}Te-^{128}Te.

those data that can be analyzed without reference to optical potentials. This discussion is based essentially on the $E2$ mixing in the "upper" levels. It allows us to determine properties of the deeply bound atomic state in an almost model independent way.

The two complex quantities $\varepsilon(6,5,j')-i\Gamma(6,5,j')/2$ for the low lying states are of interest. Equation (2) allows us to determine these complex shifts in terms of the experimental upper level values $\varepsilon(8,7,j)-i\Gamma(8,7,j)/2$ provided one is able to extract $\varepsilon(E2)-i\Gamma(E2)/2$ from the experimental data. In the given equation

$$\varepsilon(8,7,j) - i\Gamma(8,7,j)/2 = \varepsilon(E2;8,7) - i\Gamma(E2;8,7)/2$$
$$+ \varepsilon_{\text{opt}}(8,7,j) - i\Gamma_{\text{opt}}(8,7,j)/2$$
$$(3)$$

the last two terms account for the direct coupling to the annihilation channels, i.e., the part which may be described by an optical potential.

The strategy adopted to obtain $\varepsilon(E2)$ and $\Gamma(E2)$ is based on the following.

(1) The $E2$-induced shifts for ^{130}Te are large due to a quasiresonant situation with a small energy difference of 20 keV. It makes these particular shifts and widths strongly dependent upon energy and width of the deeply bound state. On the other hand, the $E2$-induced shifts for ^{128}Te down to ^{122}Te are almost independent of the properties of this state. This happens because of the large ($>$150 keV) energy mismatch. The induced level shifts for $^{128-122}$Te are calculated and displayed in Table VI. It turns out that the residual shifts, defined as experimental minus $E2$-induced shifts, are very small. These residual shifts may be attributed to the effect of an optical potential in the $n=8$ states as indicated in Eq. (3). As a next step, the optical shifts obtained in ^{128,126,124,122}Te are used to calculate a small optical potential shift for ^{130}Te. It is done by a linear regression method and the extrapolated values are given in Table VI. Now for ^{130}Te the procedure is *reversed* and the induced $E2$ shifts are calculated as the ex-

perimental minus the extrapolated optical shifts.

(2) A similar procedure is adopted for the level widths (see Table VII). An alternative procedure would be to calculate the optical components of shifts and widths in terms of an optical potential. This introduces some uncertainty related to the form of the potential and the neutron densities, which is of the order of 1 eV for the level width. It generates an uncertainty of (2–3)% to the induced width and the width of the admixed level, much smaller than the error due to other sources. However, there are difficulties in this way as the phenomenological potentials have never been tested against the upper shifts. Attractive potentials yield attractive upper shifts of the order of −0.5 eV, inconsistent with the data. Therefore, the linear regression method seems more reliable.

(3) The final step is to determine from Eq. (2) the best results for the deeply bound state (see Table VIII). Points (1) and (2) are repeated to obtain self-consistency. The errors in Table VIII correspond to the experimental errors given in Tables VI and VII. In this way one obtains two repulsive shifts in the upper and lower $j=l+1/2,l-1/2$ fine structure components and two widths of these components. Figure 6 shows that the measured width of the $n=6$ level in ^{130}Te extends smoothly the previous systematics of these widths.

It is interesting to notice a large LS effect, partly masked by the experimental errors. Qualitatively the difference in shifts is consistent with the measurements done on the $n=8$ levels in ^{174}Yb, which indicate an enhancement of the electromagnetic fine structure splitting by nuclear LS interactions [13]. On the other hand, this effect does not exist in the neighboring ^{172}Yb, ^{176}Yb nuclei [4]. Considering the level widths in the present case the LS effect is opposite to that observed in the Yb atoms. The upper width is *larger* than the lower width. This goes against a simple geometric effect due to the electromagnetic LS force. One would expect the wave function $|\Psi_-|$ at the nuclear surface to be larger than $|\Psi_+|$ as a result of LS attraction for the first and repulsion for the second state. Such an effect accounts for the Yb widths. Here in ^{130}Te however, one needs a genuine nuclear absorptive LS potential to explain the result.

TABLE VIII. Shifts and widths of the deeply bound $n,l=6,5$ level in ^{130}Te.

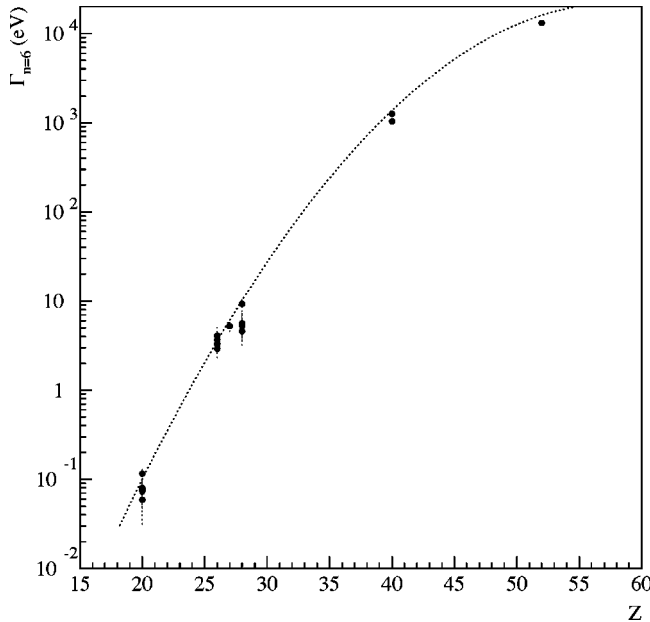| State (n,l)	Experimental ε (keV)		Experimental Γ (keV)		Calculated $\varepsilon-i\Gamma$ (keV)
(n,l)	$j=l+1/2$	$j=l-1/2$	$j=l+1/2$	$j=l-1/2$	
$(6,5)$	6.6 ± 3.8	3.6 ± 1.1	17.0 ± 4.4	11.8 ± 4.4	$6.8-i18.2$

FIG. 6. The widths of the circular $n=6$ level [2], including the deeply bound level in ^{130}Te as a function of the atomic number Z. The line interpolates the widths calculated with the optical potential used in Sec. IV B [20].

In the case of ^{122}Te, the $n=9$ level is mixed with the $n=7$ level of known shift and width. From the experimental width of 0.95(24) eV in this state and Eq. (2) one calculates the widths of the $n=7$ state to be $\Gamma=559(100)$ eV. This value exhausts, and is consistent with the line width $\Gamma=622(54)$ eV observed directly in the $n=7$ state. The other, optical contribution to the width of the $n=9$ state is insignificant ($\Gamma_{opt}\simeq 10^{-2}$ eV). This situation is visualized in Fig. 5.

A similar analysis may be performed for the lower $|n=7,l=6\rangle$ states. These states are coupled by the quadrupole interaction to a very low $|n=5,l=4\rangle$ state and this coupling generates some $E2$-induced complex shifts to the $|n=7,l=6\rangle$ states. Now, however, the analysis cannot be performed in a model independent way, since the $E2$-induced widths and shifts are smaller than the optical shifts. To calculate the effect one needs the level shift for the $n=5$ circular state, which we calculated with the optical potential discussed in the following section. One obtains $\varepsilon(n=5)\simeq 130$ keV, $\Gamma(n=5)\simeq 150$ keV, but these numbers are rather uncertain as the shape of the optical potential at the relevant radii is uncertain. The results for the induced level shifts and widths are given in Table IX. The errors are due to an estimated 50% uncertainty of ε, Γ for the $n=5$ state.

In Fig. 7 all the available data for $n=6$ antiprotonic level widths are again presented. However, to compare the real effects of nuclear absorption, the trivial consequence of atomic wave function normalization was removed, i.e., the widths were multiplied by B^{2l+3} (B – Bohr radius). This figure indicates the initial increase, saturation, and ultimate damping of the absorption that follows the increasing penetration of antiprotons into the nuclear interior. Such a behavior, typical for strongly absorptive interactions, is found in the S wave $\bar{p}$ scattering on very light nuclei [14,15] and in

TABLE IX. The $E2$-induced shifts and widths of the $n,l=7,6$ levels.

Isotope	$E2$-induced shifts (eV)		$E2$-induced widths (eV)	
	$j=l+1/2$	$j=l-1/2$	$j=l+1/2$	$j=l-1/2$
^{122}Te	−28(2)	−35(3)	3(1)	4(2)
^{124}Te	−23(2)	−30(3)	3(1)	4(2)
^{126}Te	−20(2)	−26(3)	3(1)	4(2)
^{128}Te	−18(2)	−23(3)	3(1)	4(2)
^{130}Te	−15(2)	−20(3)	3(1)	4(2)

the $n=4$ states in light $\bar{p}$ atoms [16]. In this experiment the effect is extended to ^{130}Te which offers the largest atomic-nucleus overlap observed so far.

The increasing role of absorption is apparently not the whole story in the ^{130}Te, $n=6$ level shift and width. As calculated in Ref. [8] the overlap allowed by the centrifugal barrier is large enough to support a hidden nuclear state of antiproton, although this possibility depends on uncertain strength of nuclear attraction at short distances. The existence of such a nuclear state is indicated by the Krell effect: a stronger attraction produces the more pronounced repulsion of the level [17]. Calculations [8] based on theoretical optical potentials and our results given in Table VII indicate that Krell effect may be generated in the $j=l+1/2$ fine structure state. There, the formation of nuclear-$\bar{p}$ state is assisted by the Coulomb and a nuclear LS potential. A more quantitative analysis including all the available information on the LS potential will be done separately.

B. Neutron density in the nuclear periphery

We have previously presented in detail [3] our approach to deduce the peripheral neutron density distributions from
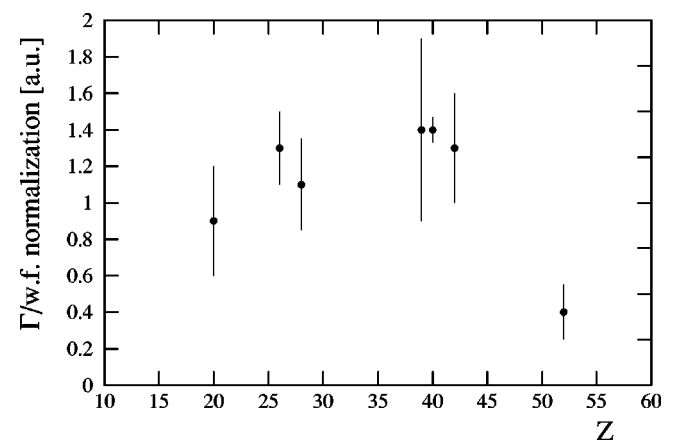

FIG. 7. The experimental widths of the circular $n=6$ level (averaged over isotopes of a given element) scaled by the normalization factor of the atomic wave function (arbitrary units) plotted vs the atomic number Z. The $Z=52$ point corresponds to the deeply bound level in ^{130}Te. Data for $Z=39$ are from Ref. [26], for $Z=42$ from Ref. [27], and other points are from Ref. [2] (see also Ref. [28]).

TABLE X. Parameters of 2pF neutron density distributions deduced from the widths of antiprotonic levels in Te atoms. c_{ch}, t_{ch}—the half-density radius and the surface thickness of charge density distributions. c_p, t_p—the half-density radius and the surface thickness of pointlike proton density distributions. Δt_{np}—difference of the surface thicknesses of proton and neutron distributions. Δr_{np}—difference of the neutron and proton rms radii.

Isotope	Charge distributions from Shera et al.[a]							Charge distributions from Fricke et al.[b]						
	c_{ch}	t_{ch}	c_p	t_p	Δt_{np}	χ^2	Δr_{np}	c_{ch}	t_{ch}	c_p	t_p	Δt_{np}	χ^2	Δr_{np}
[122]Te	5.506[c]	2.377[c]	5.546	2.087	$0.23^{+0.13}_{-0.15}$	1.3	$0.08^{+0.04}_{-0.05}$	5.5368	2.30	5.577	1.995	$0.33^{+0.11}_{-0.13}$	1.3	$0.11^{+0.04}_{-0.04}$
[124]Te	5.531	2.34	5.571	2.043	$0.20^{+0.10}_{-0.14}$	0.8	$0.06^{+0.04}_{-0.04}$	5.5503	2.30	5.590	1.995	$0.25^{+0.11}_{-0.13}$	0.8	$0.08^{+0.04}_{-0.05}$
[126]Te	5.563	2.295	5.603	1.991	$0.32^{+0.11}_{-0.13}$	1.6	$0.11^{+0.03}_{-0.05}$	5.5617	2.30	5.601	1.995	$0.32^{+0.10}_{-0.13}$	1.6	$0.10^{+0.04}_{-0.04}$
[128]Te	5.593	2.253	5.633	1.948	$0.35^{+0.13}_{-0.16}$	1.3	$0.11^{+0.04}_{-0.05}$	5.5728	2.30	5.612	1.995	$0.30^{+0.14}_{-0.17}$	1.3	$0.09^{+0.05}_{-0.05}$
[130]Te	5.622	2.209	5.661	1.894	$0.46^{+0.18}_{-0.24}$	0.3	$0.15^{+0.06}_{-0.08}$	5.5832	2.30	5.623	1.995	$0.36^{+0.18}_{-0.25}$	0.3	$0.12^{+0.06}_{-0.09}$

[a]Reference [21].
[b]Reference [23].
[c]Extrapolated values (see text).

antiprotonic x-ray data. Recently this approach was illustrated by a comparison with the Hartree-Fock-Bogoliubov model [6].

In short, the point proton and point neutron distributions are assumed to be represented by two-parameter Fermi (2pF) distributions of the form $\rho(r) = \rho_o \{1 + \exp[(r-c)/a]\}^{-1}$. Here c is the half-density radius, a the diffuseness parameter [related to the surface thickness t by $t = (4 \ln 3)a$], and ρ_0 is a normalization factor. The point proton distributions are obtained from the charge distributions, determined using electron scattering or muonic atom data. Based on our radiochemical experiments [18,19] we inferred [3] that the half-density radii of the proton and neutron distributions are almost equal. Therefore the only unknown parameter of the neutron distribution is its surface thickness. This parameter is obtained from the $\bar{p}$-atom lower and upper level widths and the lower level shift, using the optical potential "$\bar{a} \cdot \rho$" with an antiproton-nucleon effective scattering length (equal for protons and neutrons) $\bar{a} = (2.5 \pm 0.3) + i(3.4 \pm 0.3)$fm, as proposed for pointlike nucleons in Ref. [20]. The differences between experimental level widths and shifts and those calculated with the parameters of the proton distribution are attributed to the extended neutron density contribution to these observables.

The charge distribution of the [124–130]Te isotopes was determined in Ref. [21] from a simultaneous analysis of two muonic x-ray energies, $2p$-$1s$ and $3d$-$2p$, and optical isotope shift data. Fermi distribution parameters c, t and rms radii (root mean square radii) were presented there. For [122]Te no muonic data were available and only the rms charge radius value was given.

Although having only two protons outside the closed $Z = 50$ shell, tellurium nuclei are slightly deformed, with the deformation parameters β_2 varying from 0.12 to 0.18, when the mass number decreases from 130 to 122 [22]. In the data of Ref. [21] the variation of the deformation is accounted for by the change in the skin thickness t of the nuclear charge distribution. It was shown that the t parameter increases linearly with the deformation parameter β_2.

In the present work we have deduced the two Fermi charge distribution parameters c and t for [122]Te by linear

extrapolation of these values from heavier isotopes plotted as a function of β_2. The deformation parameters from Ref. [22] were used. The rms value of the charge distribution in [122]Te calculated from the extrapolated c, t values is equal to 4.715 fm, to be compared with 4.713 fm obtained from the optical isotope shift data, as quoted in Ref. [21].

In the first-half of Table X we present the 2pF charge distribution parameters, c_{ch} and t_{ch} [21], and the deduced point proton distribution parameters c_p, t_p. The neutron diffuseness, considered as a free parameter, was adjusted to get best agreement with the experimental lower and upper level widths and lower level shifts, corrected for the $E2$-resonance effect as discussed in Sec. IV B. The half-density radius parameters were assumed to be equal, $c_n = c_p$. The resulting differences $\Delta t_{np} = t_n - t_p$ and $\Delta r_{np} = r_n - r_p$ (the difference between the neutron and proton rms radii) are shown for the investigated tellurium nuclei.

Using the experimental data of Ref. [21] the charge distribution parameters of the tellurium isotopes were again listed in Ref. [23], but only the $2p$-$1s$ transition in the muonic atom was used. In this tabulation the skin thickness t was fixed at 2.3 fm for all spherical nuclei from [9]Be to [209]Bi. This procedure has apparently no noticeable effect on the rms radii of even tellurium isotopes, which agree within 0.03 fm in both references. However, at large distances both parameterizations differ significantly. This is illustrated in Fig. 8, where the charge density ratio as deduced from Ref. [21] and Ref. [23] are shown for [122]Te and [130]Te, respec-
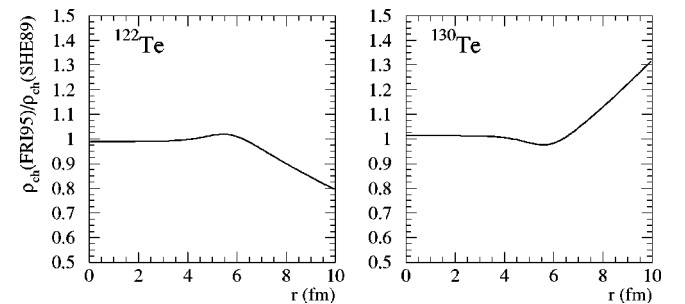

FIG. 8. Comparison of the charge density distribution deduced from the two-parameter Fermi distribution of Refs. [21,23].
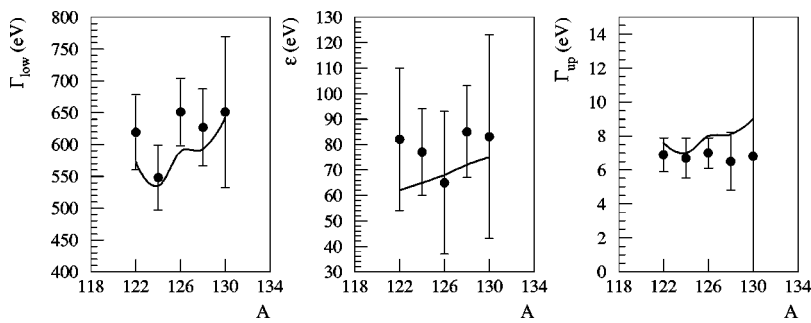
FIG. 9. Average widths and shifts of the level $(n,l=7,6)$ and widths of the level $(n,l=8,7)$ plotted vs A in the tellurium isotopes. Upper level widths and lower level shifts are corrected for the $E2$ effect. The lines are calculated using the optical potential for pointlike nucleons [20] with the surface parameters given in Table X (see also text). Positive level shifts correspond to repulsive interactions.

tively. For ^{122}Te at large distance the charge density from Ref. [23] is smaller than that from Ref. [21]. For ^{130}Te isotope the situation is reversed.

The deduced differences between neutron and proton rms values using charge distributions from Ref. [23] are shown in the second-half of Table X. Although the deduced Δr_{np} values agree within the quoted errors with those obtained for the charge distributions of Ref. [21], no isotope effects can be discerned. We continue our discussion of the neutron distribution in tellurium nuclei basing on the charge distribution parameters given in Ref. [21].

Using bare-proton and bare-neutron distributions as listed for the tellurium isotopes in the first-half of Table X and using the scattering lengths given above, the theoretical widths and shifts were compared with the experimental ones and are presented in Fig. 9. It is evident that the potential used is able to reproduce, within the experimental errors, the lower and upper level widths and the lower-level shift.

The analysis of the x-ray data as presented in Table X allows us to determine the normalized neutron to proton density ratio $(Z\rho_n)/(N\rho_p)$ as a function of the radial distance at the periphery of the investigated even tellurium isotopes. This ratio is presented in Fig. 10. As previously discussed [3], the radiochemical experiment [24] can be considered as giving the same ratio at a radial distance around 2.5 fm larger than the charge density radius. The radiochemical experiment was performed [18] for the isotopes ^{128}Te and ^{130}Te and its results are also shown in Fig. 10. The experimental data are compared with the proton to neutron density ratio obtained from spherical Hartree-Fock-Bogoliubov (HFB) calculations [25]. The difference between theoretical and experimental density distributions increases with decreasing tellurium mass number, what may be due to the neglect of deformation in the calculated densities.

Finally, in Fig. 11 the differences Δr_{np} between neutron and proton rms radii for tellurium isotopes are plotted as a function of the nuclear asymmetry parameter $\delta=(N-Z)/A$. They are compared with our previous systematics of Δr_{np} values given in Ref. [3]. It is worth mentioning that for the previous systematics only ^{128}Te was used.
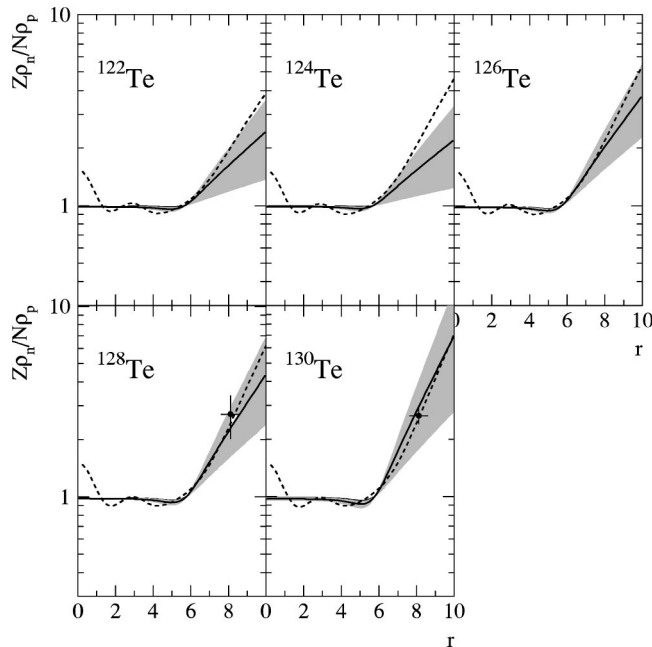

FIG. 10. Normalized neutron-to-proton density ratio $(Z\rho_n)/(N\rho_p)$ deduced from strong-interaction level widths and shifts (solid lines with indicated statistical errors) and charge distributions given in Ref. [21]. They are compared with f_{halo} measured in the radiochemical experiment (marked with crosses at a radial distance corresponding to the most probable annihilation site) and with HFB model calculations (dashed lines).
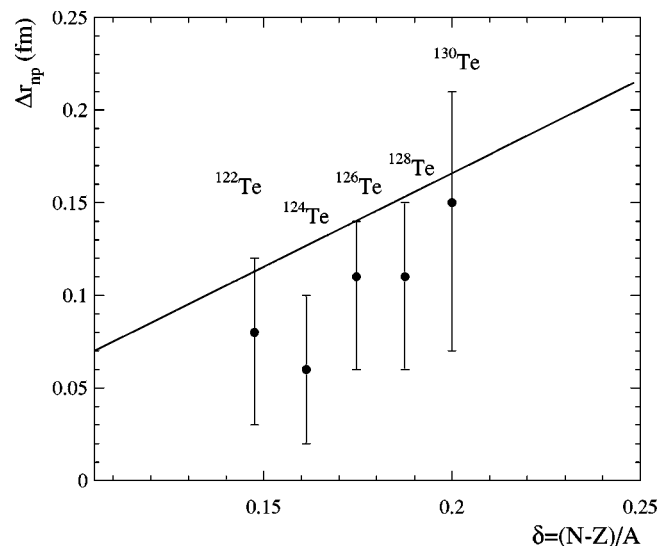

FIG. 11. Difference Δr_{np} between the rms radii of the neutron and proton distributions as deduced from the antiprotonic atom x-ray data and charge distributions from Ref. [21], as a function of $\delta=(N-Z)/A$. The full line is the same as in Fig. 4 of Ref. [3].

V. SUMMARY AND CONCLUSIONS

Antiprotonic x-ray were measured in five even tellurium isotopes. The strong interaction level widths and shifts were determined. These observables are strongly affected by the $E2$ mixing of nuclear and atomic states. The analysis of the $E2$ resonance occurring in ^{130}Te allowed to deduce the widths and shifts of the deeply bound level $n, l = 6, 5$, which cannot be directly observed. The LS splitting of its components gives clear evidence of a strong nuclear spin-orbit force contribution to the determined widths and shifts of this level. Till now there exists only conflicting evidence [4,13] on the observation of this effect in Yb isotopes. We believe that the ^{130}Te case opens a new interesting topic for further research.

The measured lower and upper level widths and lower level shifts, corrected for the $E2$ effects, were used to determine the properties of the nuclear periphery. We have assumed that the simple two-parameter Fermi model describes the peripheral proton and neutron distributions. The 2pF point proton distributions were taken from muonic-atom experiments. Based on our radiochemical experiments it was assumed that the half-density radii of the proton and neutron distributions are the same. The neutron distribution diffuseness was adjusted to account best for the experimental level widths and shifts. The neutron rms radius obtained in this way was used to determine the difference between the neutron and the proton rms radii, Δr_{np}. This difference exhibits a dependence on the mass number and is in reasonable agreement with Δr_{np} values determined previously for a wide mass number range [3].

[1] A. Trzcińska, J. Jastrzębski, T. Czosnyka, T. von Egidy, K. Gulda, F. J. Hartmann, J. Iwanicki, B. Ketzer, M. Kisieliński, B. Kłos, W. Kurcewicz, P. Lubiński, P. Napiorkowski, L. Pieńkowski, R. Schmidt, and E. Widmann, Nucl. Phys. **A692**, 176c (2001).

[2] A. Trzcińska, J. Jastrzębski, P. Lubiński, F. J. Hartmann, R. Schmidt, T. von Egidy, and B. Kłos, Acta Phys. Pol. B **32**, 917 (2001).

[3] A. Trzcińska, J. Jastrzębski, P. Lubiński, F. J. Hartmann, R. Schmidt, T. von Egidy, and B. Kłos, Phys. Rev. Lett. **87**, 082501 (2001).

[4] R. Schmidt, F. J. Hartmann, T. von Egidy, T. Czosnyka, J. Iwanicki, J. Jastrzębski, M. Kisieliński, P. Lubiński, P. Napiorkowski, L. Pieńkowski, A. Trzcińska, J. Kulpa, R. Smolańczuk, S. Wycech, B. Kłos, K. Gulda, W. Kurcewicz, and E. Widmann, Phys. Rev. C **58**, 3195 (1998).

[5] F. J. Hartmann, R. Schmidt, B. Ketzer, T. von Egidy, S. Wycech, R. Smolańczuk, T. Czosnyka, J. Jastrzębski, M. Kisieliński, P. Lubiński, P. Napiorkowski, L. Pieńkowski, A. Trzcińska, B. Kłos, K. Gulda, W. Kurcewicz, and E. Widmann, Phys. Rev. C **65**, 014306 (2002).

[6] R. Schmidt, A. Trzcińska, T. Czosnyka, T. von Egidy, K. Gulda, F. Hartmann, B. Ketzer, M. Kisieliński, B. Kłos, W. Kurcewicz, P. Lubiński, P. Napiorkowski, L. Pieńkowski, R. Smolańczuk, E. Widmann, and S. Wycech, Phys. Rev. C **67**, 044308 (2003).

[7] M. Leon, Nucl. Phys. **A260**, 461 (1976).

[8] S. Wycech, F. J. Hartmann, H. Daniel, W. Kanert, H. S. Plendl, T. von Egidy, J. J. Reidy, M. Nicholas, L. A. Redmond, H. Koch, A. Kreissl, H. Poth, and D. Rohmann, Nucl. Phys. **A561**, 607 (1993).

[9] E. Borie, Phys. Rev. A **28**, 555 (1983).

[10] Y. Eisenberg and D. Kessler, Nuovo Cimento **19**, 1195 (1961).

[11] R. A. Ferrell, Phys. Rev. Lett. **4**, 425 (1960).

[12] S. Devons and I. Duerdoth, Adv. Nucl. Phys. **2**, 295 (1969).

[13] A. Kreissl, A. D. Hancock, H. Koch, T. Köhler, H. Poth, U. Raich, D. Rohmann, A. Wolf, L. Tauscher, A. Nilsson, M. Suffert, M. Chardalas, S. Dedoussis, H. Daniel, T. von Egidy, F. J. Hartmann, W. Kanert, H. Plendl, G. Schmidt, and J. J. Reidy, Z. Phys. A **329**, 235 (1988).

[14] K. Protasov, G. Bonomi, E. L. Rizzinoi, and A. Zenoni, Eur. Phys. J. A **7**, 429 (2000).

[15] A. Gal, E. Friedman, and C. Batty, Phys. Lett. B **491**, 219 (2000).

[16] A. Green and S. Wycech, Nucl. Phys. **A467**, 744 (1987).

[17] M. Krell, Phys. Rev. Lett. **26**, 584 (1971).

[18] P. Lubiński, J. Jastrzębski, A. Trzcińska, W. Kurcewicz, F. J. Hartmann, W. Schmid, T. von Egidy, R. Smolańczuk, and S. Wycech, Phys. Rev. C **57**, 2962 (1998).

[19] R. Schmidt, F. J. Hartmann, B. Ketzer, T. von Egidy, T. Czosnyka, J. Jastrzębski, M. Kisieliński, P. Lubiński, P. Napiorkowski, L. Pieńkowski, A. Trzcińska, B. Kłos, R. Smolańczuk, S. Wycech, W. Pöschl, K. Gulda, W. Kurcewicz, and E. Widmann, Phys. Rev. C **60**, 054309 (1999).

[20] C. J. Batty, E. Friedman, and A. Gal, Nucl. Phys. **A592**, 487 (1995).

[21] E. B. Shera, M. V. Hoehn, G. Fricke, and G. Mallot, Phys. Rev. C **39**, 195 (1989).

[22] S. Raman, C. H. Malarkey, W. T. Milner, C. W. Nestor, Jr., and P. H. Stelson, At. Data Nucl. Data Tables **36**, 1 (1987).

[23] G. Fricke, C. Bernhardt, K. Heilig, L. A. Schaller, L. Schellenberg, E. B. Shera, and C. W. de Jager, At. Data Nucl. Data Tables **60**, 177 (1995).

[24] J. Jastrzębski, H. Daniel, T. von Egidy, A. Grabowska, Y. S.

Kim, W. Kurcewicz, P. Lubiński, G. Riepe, W. Schmid, A. Stolarz, and S. Wycech, Nucl. Phys. **A558**, 405c (1993).

[25] R. Smolańczuk (private communication).

[26] P. Robertson, T. King, R. Kunselman, J. Miller, R. J. Powers, P. D. Barnes, R. A. Eisenstein, R. B. Sutton, C. R. Cox, M. Eckhause, J. R. Kane, A. M. Rushton, W. F. Vulcan, and R. E. Welsh, Phys. Rev. C **16**, 1945 (1977).

[27] W. Karnet, F. J. Hartmann, H. Daniel, E. Moser, G. Schmidt, T. von Egidy, J. J. Reidy, M. Nicholas, M. Leon, H. Poth, G. Büche, A. D. Hancock, H. Koch, Th. Köhler, A. Kreissl, U. Raich, D. Rohmann, M. Chardalas, S. Dedoussis, M. Suffert, and A. Nilsson, Phys. Rev. Lett. **56**, 2368 (1986).

[28] S. Wycech, Nucl. Phys. **A692**, 29c (2001).